ISSN 1995-0802, Lobachevskii Journal of Mathematics, 2023, Vol. 44, No. 10, pp. 4489–4497. © Pleiades Publishing, Ltd., 2023.

Lattice Boltzmann Simulations of the Dynamic Adsorption of Gas in Porous Media: Effect of Grain Size Distribution

T. R. Zakirov[1,2*], M. G. Khramchenkov[1,2], A. N. Kolchugin[1***], and A. A. Galeev[1****]**

(Submitted by A. M. Elizarov)

[1] *Institute of Geology and Petroleum Technologies, Kazan Federal University, Kazan, 420008, Russia*

[2] *Kazan Branch of Joint Supercomputer Center, Scientific Research Institute of System Analysis, Russian Academy of Sciences, Kazan, 420111, Russia*

Received June 16, 2023; revised July 12, 2023; accepted August 01, 2023

Abstract—This paper presents a study of the dynamic adsorption of gas (methane) with single-phase flows in porous media. The purpose is to determine the effect of grain size distribution on dynamic adsorption at different ratios between inter- and intraparticle diffusion coefficients. The findings of this paper have been obtained using lattice Boltzmann equations and "computational rock physics" technology, which involves numerical simulations on binary images of porous structures. The results showed that grain size distribution and the ratio between inter- and intraparticle diffusion coefficients are factors affecting dynamic adsorption. It has been established that at low ratios between diffusion coefficients, dynamic adsorption is determined by surface adsorption and does not depend on grain size distribution. At high ratios, an increase in the standard deviation contributes to a slowdown in the total dynamic adsorption. In addition, it has been found that an increase in the variety of grain sizes promotes a significant decrease in the prediction reliability of the adsorption dynamics.

DOI: 10.1134/S1995080223100463

Keywords and phrases: *dynamic adsorption; surface reaction; grain size distribution; lattice Boltzmann equations; digital core.*

1. INTRODUCTION

The processes of dynamic adsorption in porous media take place in many industrial and engineering applications, such as catalysis, underground fluid mechanics, soil science, enhanced hydrocarbon recovery, and many others. In this paper, we focus on studying the dynamic adsorption of gas component with single-phase flows in porous media. Understanding the mechanisms of gas adsorption (for example, CH_4, CO_2, N_2) is essential for many problems, such as enhanced recovery methods in shales and coals [1, 2] and CO_2 sequestration [3].

To date, a lot of experience has been accumulated in the field of studying mass transfer processes in porous media with single-phase flows. During numerical and physical experiments, it has been found that porosity, temperature, flow rate, concentration, and adsorption rate constant are the factors that strongly influence the dynamic adsorption of gas [4–9]. It has been established that their increase stimulates adsorption dynamics. On the contrary, the Peclet number, the pore space heterogeneity, and the particle number are factors whose increase contributes to the suppression of the adsorption dynamics [5, 7, 10]. According to [10], absolute permeability has no effect on dynamic adsorption.

The mass transfer processes between gases and adsorbent particles involve two stages [6, 7]. First, is the interparticle adsorption, which includes the gas transport in the pore space, as well as the surface

*E-mail: tirzakirov@kpfu.ru
**E-mail: mkhramch@gmail.com
***E-mail: anton.kolchugin@gmail.com
****E-mail: agaleev@kpfu.ru

reaction on the outer surface of the particle. This process is defined by the flow rate, adsorption and desorption rate constants, as well as the interparticle diffusion coefficient. Gas being adsorbed on the particle surface has the ability to penetrate inside the particle through diffusion mechanisms. This is the second stage, called intraparticle or total adsorption, which is determined by the intraparticle diffusion coefficient.

In this paper, the adsorption process is studied using mathematical modeling based on the lattice Boltzmann equations (abbreviated as LBEs) [11]. According to "Computational rock physics" approach, flow simulations are performed on binary images of porous structures, in which cells belong to the pore or solid phase [12]. The advantage of the LBEs in comparison with the family of models based on the Navier–Stokes equations is the absence of the need to solve the system of linear algebraic equations each time step, which significantly speeds up the solution and simple boundary conditions on solid surfaces [13], high efficiency of program code parallelization [14], easy implementation of the convective-diffusion equation for the dissolved component and simple modeling of mass transfer on the active component/adsorbent interface [15].

In this paper, we investigate the dynamic adsorption of gas (methane) with single-phase flows in porous media. The main scope is to reveal the effect of grain size distribution on dynamic adsorption at different ratios between inter- and intraparticle diffusion coefficients. The results have been obtained using lattice Boltzmann simulations performed on two-dimensional synthetic digital images of porous media. In addition, special attention is paid to establishing the prediction accuracy of the dynamic adsorption depending on the grain size distribution based on a series of numerical simulations.

2. METHODS

2.1. Mathematical Model

The mathematical model consists of the following parts: governing equations for a single-phase fluid flow (Section 2.1.1); model for convective diffusion of the dissolved component (Section 2.1.2); equations describing surface reactions and diffusion inside the adsorbent particles (Section 2.1.3). Some parts of this model have already been published in [10, 12]. In the presented paper, we provide a brief description of the mathematical statement using references.

2.1.1. Governing equations for fluid flow. Fluid flow is described using the lattice Boltzmann equations. The variables such as time- and space-dependent pressure and velocity are calculated using the distribution functions $f_i(\mathbf{r}, t)$ [11], where index i determines the direction of particles' motion during the time step Δt. In this paper, we consider D2Q9 lattice, which defines the velocity basis as: $\mathbf{e}_1 = c \cdot (0,0)$, $\mathbf{e}_2 = c \cdot (1,0)$, $\mathbf{e}_3 = c \cdot (0,1)$, $\mathbf{e}_4 = c \cdot (-1,0)$, $\mathbf{e}_5 = c \cdot (0,-1)$, $\mathbf{e}_6 = c \cdot (1,1)$, $\mathbf{e}_7 = c \cdot (-1,1)$, $\mathbf{e}_8 = c \cdot (-1,-1)$, $\mathbf{e}_9 = c \cdot (1,-1)$, where Δl is the grid step, and $c = \Delta l / \Delta t$ is the lattice speed.

The evolution of f_i in time and space is described by [10]

$$f_i(\mathbf{r} + \mathbf{e}_i \Delta t, t + \Delta t) = f_i(\mathbf{r}, t) + \Omega_i(\mathbf{r}, t). \tag{1}$$

Equation (1) is solved in two stages. The first step is the particles' streaming, in which they move towards neighboring nodes in the directions $\mathbf{e}_i$ ($i = 1$–9). The second stage is the calculation of the collision operator Ω_i. In the LBEs, the macroscopic variables are density (pressure equivalent) and velocity, calculated from equations

$$\rho_i(\mathbf{r}, t) = \sum_{i=1}^{9} f_i(\mathbf{r}, t), \quad \mathbf{u}(\mathbf{r}, t) = \frac{1}{\rho} \sum_{i=1}^{9} \mathbf{e}_i f_i(\mathbf{r}, t).$$

Fluid pressure and density are related as $P = \rho c^2/3$. The relationship between kinematic viscosity η (m^2/s) and Δt is established using the relaxation parameter τ_f for fluid flow as [11]

$$\eta = \left(\frac{2\tau_f - 1}{6} \right) \frac{\Delta l^2}{\Delta t}.$$

The collision operator Ω_i in Eq. (1) is described using the Multi-relaxation time (MRT) scheme [13]

$$\Omega_i = -\mathbf{M}^{-1} \mathbf{S} (m_i - m_i^{eq}).$$

Moments $m = (\rho, e, \epsilon, j_x, q_x, j_y, q_y, p_{xx}, p_{xy})^T$ are calculated as $m_i = \sum_{k=1}^{9} \mathbf{M}_{ik} f_k$. Matrix $\mathbf{M}$, the equations for the equilibrium moments m^{eq}, and the collision matrix $\mathbf{S}$ are given in [13].

Boundary conditions on the impermeable surfaces are realized using "bounce-back" conditions [11]: $f_i(\mathbf{r}, t + \Delta t) = f^*_{i_{opp}}(\mathbf{r}, t)$. The sign * characterizes the state after particles' collision. The indices i and i_{opp} indicate opposite directions.

2.1.2. Governing equations for convective diffusion transport of gas. In this paper, the gas concentration in the injected fluid is low that its effect on the fluid flow is negligible. Gas concentration is determined by the distribution functions g_l, the evolution of which is written as [6, 7]

$$g_l(\mathbf{r} + \mathbf{e}_l \Delta t, t + \Delta t) = g_l(\mathbf{r}, t) - \frac{1}{\tau_s}[g_l(\mathbf{r}, t) - g_l^{eq}(\mathbf{r}, t)], \tag{2}$$

where τ_s is the relaxation parameter for gas, and g_l^{eq} is the equilibrium distribution function. The collision scheme is presented by a Single-relaxation time model due to reduction in computational costs. For gas transport, we use D2Q5 lattice without loss of the results' accuracy [10]. In the D2Q5 lattice, only the first five vectors from the D2Q9 lattice are considered.

Gas concentration C and the relaxation parameter τ_s are calculated using the following formulas [6, 7]

$$C(\mathbf{r}, t) = \sum_{l=1}^{5} g_l(\mathbf{r}, t), \quad \tau_s = 0.5 + 3\,\frac{D_s\,\Delta t}{\Delta t^2},$$

where D_s is the interparticle diffusion coefficient. The equilibrium distribution functions in Eq. 2 are described as

$$g_l^{eq}(\mathbf{r}, t) = \tilde{w}_l C \left[1 + \frac{(\mathbf{e}_l \cdot \mathbf{u})}{C^2}\right],$$

where $\tilde{w}_1 = 1/3$, $\tilde{w}_{2-5} = 1/6$ are the weight coefficients.

The boundary conditions at the particle surface are described as [15]

$$\sum_{l=1}^{5} g_l \mathbf{e}_l = -D_s \nabla C.$$

2.1.3. Surface reaction and diffusion inside particles. The adsorption process includes two types: mass transfer on the outer surface (surface reaction) and the diffusion inside particles in nano-porous channels (intraparticle diffusion). Surface reaction is described by the kinetic equation of the Langmuir adsorption [6, 7, 10, 12]

$$D_s \frac{\partial C_w}{\partial \mathbf{n}} = \frac{\partial N^{surf}}{\partial t} = [k^a C_w (N^{max} - N^{surf}) - k^d N^{surf}], \tag{3}$$

where k^a and k^d are the adsorption and desorption rate constants, respectively; N^{surf} is the adsorbed amount on the particles surface; N^{max} is the maximum adsorbed amount; $\mathbf{n}$ is the normal vector to the solid surface.

The diffusion mechanics inside the particles is described by the second Fick's law

$$\frac{\partial N^{total}}{\partial t} = D_{sp} \Delta N^{total},$$

where N^{total} is the adsorbed amount inside particles. When solving Eq. 3, N^{surf} is defined on the particles' surface and used as boundary condition.

In this paper, we study both surface adsorbed amount and the adsorption amount inside the particles, called total adsorption. These parameters are presented in dimensionless form. Surface adsorbed amount $N_t^{surf}(i, j)$, calculated at the time t in computational node (i, j), is averaged over all computational nodes belonging to the particles surface and is normalized to the maximum adsorbed value

$$\overline{N_t^{surf}} = \frac{\sum_{i,j} N_t^{surf}(i, j)}{W^{surf}\, N^{max}},$$

Table 1. Properties of digital images of porous media with various grain size distributions

Sample number	Porosity, rel. units	Specific surface area, mm^{-1}	Absolute permeability, k_{XX}, mkm^2	Grain size distribution	
				Average radius, mkm	Standard deviation, σ, mkm
1	0.631	0.088	7.44	20	0
2	0.627	0.088	8	20	1.26
3	0.630	0.087	7.96	20	2.1
4	0.641	0.088	6.52	20	2.68
5	0.634	0.089	6.48	20	3.68
6	0.630	0.086	4.28	20	3.98
7	0.632	0.087	6.08	20	4.72
8	0.634	0.087	5.1	20	5.25

where W^{surf} is the total number of nodes at the particles surface. The dimensionless total adsorbed amount is calculated as

$$\overline{N_t^{total}} = \frac{\sum_{i,j} N_t^{total}(i,j)}{W^{total}\, N^{max}}. \tag{4}$$

In Eq. 4, (i, j) belong to the nodes inside particles, excluding nodes on the surface; W^{total} is the total number of nodes associated with the adsorbent particles.

2.2. Flow Regions and Simulation Parameters

The numerical simulations are performed on synthetic digital models of porous media. In this paper, we study the effect of grain size distribution on dynamic adsorption. To generate porous structures with a controlled grain size distribution, the Monte-Carlo movement method is applied [16]. Examined grain size distributions obey normal distribution laws with the same average value and different standard deviations. The flow regions have close values of porosity and specific surface area to avoid the effect of these parameters on dynamic adsorption [12]. Properties of porous structures are listed in Table 1 and images of digital cores with various grain size distributions are shown in Fig. 1. The size of digital images is 960×540 lattice units (l.u.).

In this paper, we study the adsorption of gas in the form of molecules of methane dissolved in the injected water vapor. At the initial time, the pore space is filled with water vapor, which does not contain gas. Water vapor with dissolved gas is injected through the inlet boundary perpendicular to the OX axis with a known flow rate u_0 and gas concentration C_0. At the outlet boundary, $P = P_{out}$ and $\partial C/\partial x = 0$. External upper and lower boundaries are impermeable and do not react with gas: $\partial C/\partial y = 0$. The adsorbent particles are selected in the form of Cu-benzene-1,3,5-tricarboxylic acid (Cu-BTC) particles [4]. Simulations are stopped when $\overline{N^{total}} = 0.9$.

The initial molar concentration of methane is 50 mol/m^3. The density ρ and kinematic viscosity η of water vapor is 0.65 kg/m^3 and 1×10^{-5} m^2/s, respectively. To avoid the effect of the flow rate [10], all simulations are performed at the same $u_0 = 0.5$ mm/s. Adsorption and desorption rate constants (k^a and k^d) are 2.5×10^3 $m^3/(mol{\cdot}s)$ and 5×10^3 s^{-1}, respectively [4]. The maximum adsorbed amount N^{max} is set 150 mol/m^3. Interparticle diffusion coefficient D_s of gas is 20×10^{-6} m^2/s. The intraparticle diffusion coefficient D_{sp} takes the following values: 0.1, 0.04, 0.02, 0.006, and 0.003×10^{-6} m^2/s.

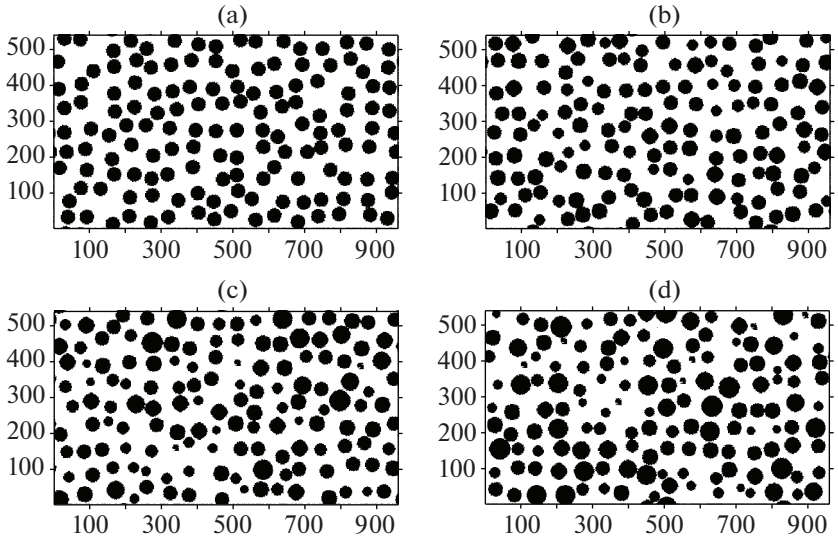

Fig. 1. Digital images of porous media with different grain size distributions: a — $\sigma = 0$ mkm; b — $\sigma = 2.1$ mkm; c — $\sigma = 3.98$ mkm; d — $\sigma = 5.25$ mkm. Black indicates solid phase, white is the pore space.

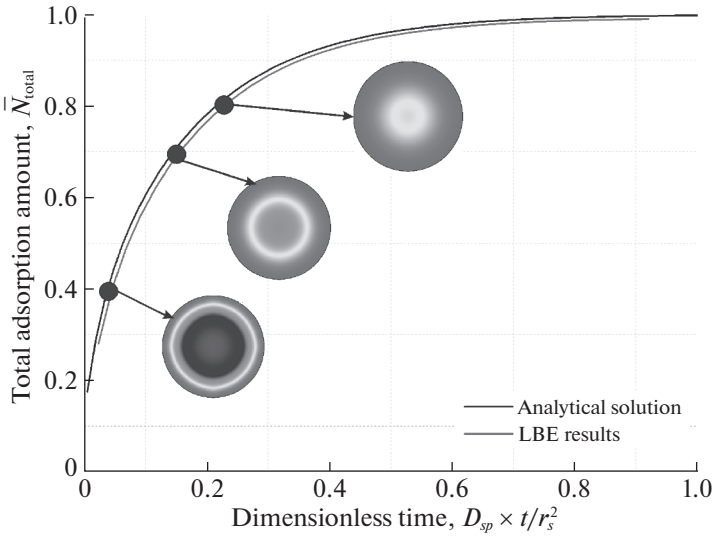

Fig. 2. Time evolution of static adsorption in a round particle. Comparison of analytical solution and LBEs results.

3. RESULTS AND DISCUSSION

3.1. Validation Test

The mathematical model formulated in the presented paper has already been validated on benchmarks in our previous works [10, 12]. Also, the results obtained with double grid refinement are close to being independent of the grid detailing. In this section, we provide an additional verification test on the static adsorption inside a round particle placed in a steady field of a uniformly distributed gas concentration. For this statement, static adsorption inside particle is described as follows [6]

$$\overline{N^{total}} = 1 - \sum_{n-1}^{\infty} \frac{4}{r_s^2\,\alpha_n^2}\,\exp(-D_{sp}\alpha_n^2 t).$$

In simulations, $D_{sp} = 1 \times 10^{-8}$ m^2/s, $r_s = 75$ mkm (particle radius), α_n is the positive root of the Bessel function of the first type of order zero $J_0(r_s\,\alpha_n)$. Only the first three roots have a significant influence on the solution: $r_s\alpha_1 = 2.405$, $r_s\alpha_2 = 5.52$, and $r_s\alpha_3 = 8.654$. The following boundary

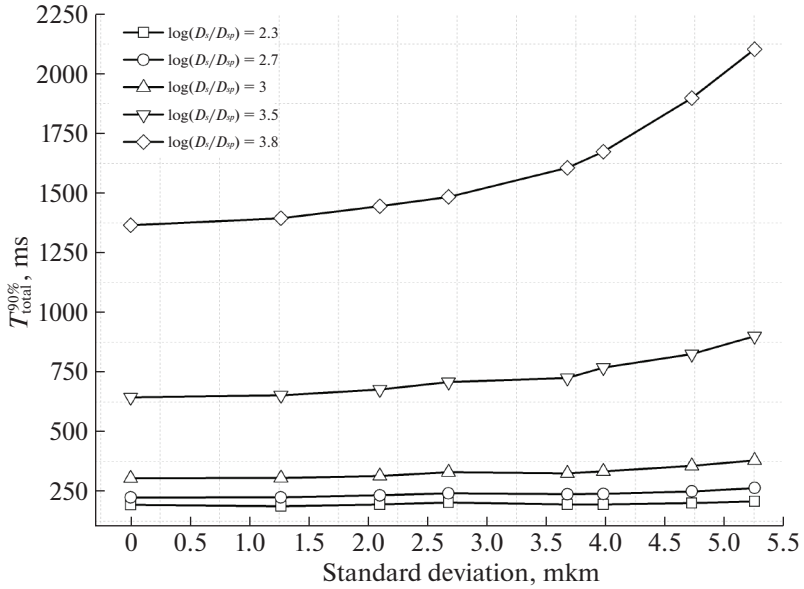

Fig. 3. The relationships between $T^{90\%}_{total}$ and standard deviation at various $\lg(D_s/D_{sp})$.

conditions are applied: $N^{total}\mid_{r=r_s} = N^{max} = 250$ mol/m^3 and $\frac{\partial N^{total}}{\partial t}\mid_{r=0} = 0$. The time evolution of static adsorption, obtained by the analytical solution and the LBEs simulations, is shown in Fig. 2. A comparison of the curves reveals satisfactory agreement between the numerical and analytical results.

3.2. Effect of Grain Size Distribution

In this section, we study the effect of grain size distributions on the dynamic adsorption of gas. The adsorption process has been investigated in terms of its dependence on the ratio between the coefficients of inter- and intraparticle diffusion. For the values given in the previous section, $\lg(D_s/D_{sp})$ ranges from 2.3 to 3.8. To evaluate the adsorption dynamics, we use the time denoted as $T^{90\%}_{total}$, at which $\overline{N^{total}_t} = 0.9$.

Figure 3 shows the relationships between $T^{90\%}_{total}$ and σ obtained for different $\lg(D_s/D_{sp})$. It has been found that an increase in $\lg(D_s/D_{sp})$, which characterizes a decrease in the intraparticle diffusion, contributes to a significant slowdown in the dynamic adsorption, which, in general, is expected and consistent with [6, 12]. The most interesting result in Fig. 3 is that $\lg(D_s/D_{sp})$ strongly impacts the relationship between $T^{90\%}_{total}$ and grain size distribution. Based on the obtained data, at low values of $\lg(D_s/D_{sp}) = 2.3$, 2.7, and 3, dynamic adsorption is practically unaffected by σ. The noticeable effect of grain size distribution has been detected at medium $\lg(D_s/D_{sp}) = 3.5$, which is characterized by an increase in $T^{90\%}_{total}$ with increasing σ. By changing σ, $T^{90\%}_{total}$ varies from 640 to 850 ms (32%). With a further increase in $\lg(D_s/D_{sp}) = 3.8$, the influence of grain size distribution on $T^{90\%}_{total}$ becomes stronger: $T^{90\%}_{total}$ ranges from 1360 to 2120 ms (56%).

To analyze the revealed trends, let's consider the relationships between surface $\overline{N^{surf}}$ and $\overline{N^{total}}$ adsorbed amounts shown for various σ and at low $\lg(D_s/D_{sp}) = 2.3$ (Fig. 4a) and high $\lg(D_s/D_{sp}) = 3.8$ (Fig. 4b). The condition $\overline{N^{total}} < \overline{N^{surf}}$ found for both $\lg(D_s/D_{sp})$ indicates the delay of total adsorption with respect to surface adsorption. It should be noted that cases of low $\lg(D_s/D_{sp})$ are characterized by fast intraparticle diffusion. According to Fig. 4a, the trends practically coincide and $\overline{N^{total}} \approx \overline{N^{surf}}$. This relation characterizes the close dynamics of total and surface adsorption. Thus, due to the fast intraparticle diffusion, the total adsorption dynamics is limited to surface adsorption. Figure 5 shows the dependence between the ratio $T^{90\%}_{total}/T^{90\%}_{surf}$ and standard deviation at low values of $\lg(D_s/D_{sp})$, where $T^{90\%}_{surf}$ is the time at which $\overline{N^{surf}_t} = 0.9$. Based on the obtained data, the ratios

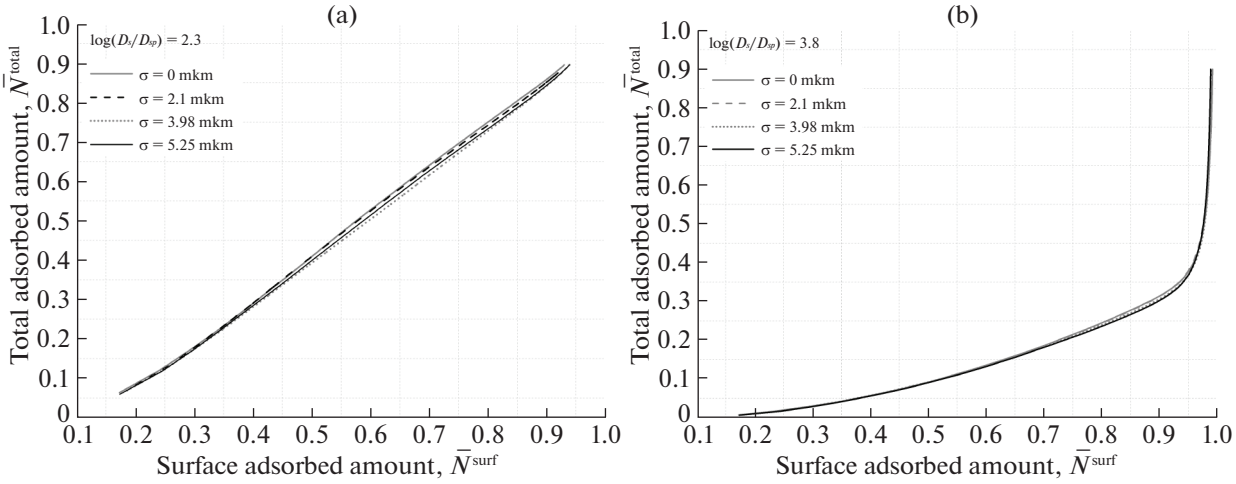

Fig. 4. The relationships between the surface $\overline{N^{surf}}$ and total $\overline{N^{total}}$ adsorbed amount at various standard deviations: a — $\lg(D_s/D_{sp}) = 2.3$; b — $\lg(D_s/D_{sp}) = 3.8$.

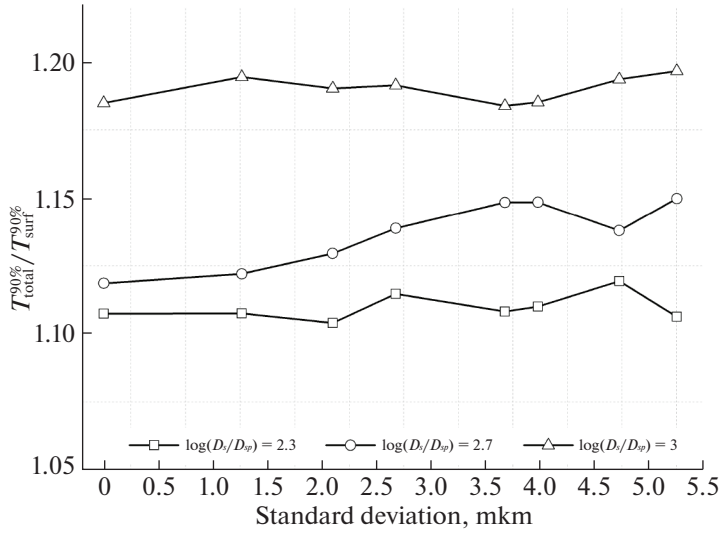

Fig. 5. The dependence between the ratio $T^{90\%}_{total}/T^{90\%}_{surf}$ and standard deviation at various $\lg(D_s/D_{sp})$.

$T^{90\%}_{total}/T^{90\%}_{surf}$ do not depend on σ and are within 1.1–1.2. This result indicates that for low $\lg(D_s/D_{sp})$, regardless of σ, $T^{90\%}_{total}$ is mainly determined by $T^{90\%}_{surf}$. This statement explains the relationship between $T^{90\%}_{total}$ and σ in Fig. 3.

In the case of a high $\lg(D_s/D_{sp}) = 3.8$ (Fig. 4b), which characterizes slow intraparticle diffusion, $\overline{N^{total}} \ll \overline{N^{surf}}$. As shown, the curves coincide. This relation means that the total adsorption dynamics is much slower than the gas convective-diffusion transport in the pore space. For such conditions, $\overline{N^{total}}$ is weakly affected by $\overline{N^{surf}}$ and is mainly determined by the intraparticle diffusion coefficient. According to Fig. 3, a negative effect of standard deviation on the dynamic adsorption has been found for this case.

Another problem stated in this paper is to evaluate the prediction reliability of the adsorbed amount of gas in dependence on grain size distribution. Prediction accuracy is numerically described using the coefficient of variation (CV) calculated based on a series of numerical experiments performed on a group of 20 different porous structures. Each group has the same grain size distribution. The simulations have

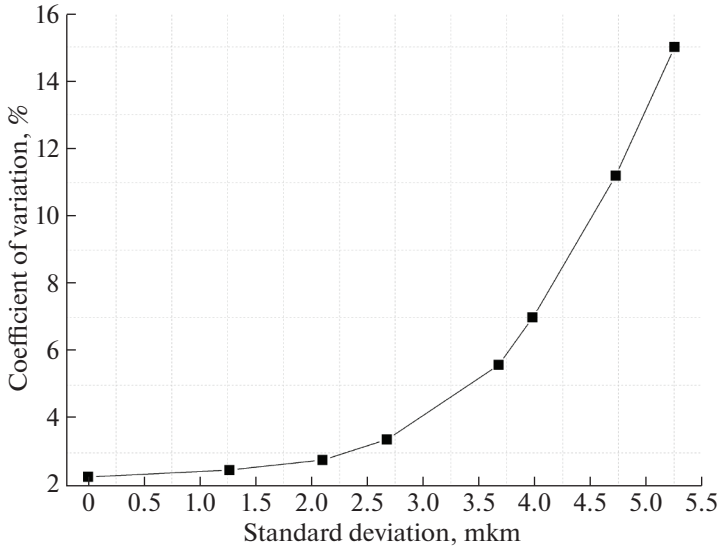

Fig. 6. Coefficient of variation of the adsorbed amount of gas versus standard deviation of grain size distribution. The results are presented for $\lg(D_s/D_{sp}) = 1000$.

been carried out for $\lg(D_s/D_{sp}) = 1000$ and stopped when $\overline{N^{total}} = 0.9$. The examined flow regions have the same size of 960×540 l.u.

The results are shown in Fig. 6. It has been established that there is a direct relationship between the standard deviation and the coefficient of variation. By changing σ, the coefficients of variation vary from 2.2 to 15%. This result indicates that as the variety of grain sizes increases, the prediction accuracy of the adsorbed amount reduces significantly.

4. CONCLUSIONS

Below, the best findings of this paper are formulated:

1. Grain size distribution and the coefficients of inter- and intraparticle diffusion are factors affecting dynamic adsorption. The sensitivity of total dynamic adsorption to changes in the grain size distribution increases with increasing $\lg(D_s/D_{sp})$ coefficients:

   a) at low $\lg(D_s/D_{sp})$, total dynamic adsorption is limited by surface adsorption and does not depend on grain size distribution;

   b) at high $\lg(D_s/D_{sp})$, an increase in the standard deviation contributes to a slowdown in the total dynamic adsorption.

2. The standard deviation of grain size distribution affects the prediction accuracy of the adsorbed amount. It has been found that an increase in the variety of grain sizes promotes a significant decrease in prediction reliability.

FUNDING

This work was funded by the subsidy allocated to Kazan Federal University for the state assignment in the sphere of scientific activities, project no. FZSM-2023-0014, and partially supported by the Joint Supercomputer Center of the Russian Academy of Sciences (Branch of Federal State Institution Scientific Research Institute for System Analysis of the Russian Academy of Sciences).

REFERENCES

1. L. Ma and Q. Yu, "Dynamic behaviors of methane adsorption on partially saturated shales," J. Pet. Sci. Eng. **190**, 107071 (2020).
2. H. Wang, X. Yang, F. Du, G. Wang, Y. Wang, W. Zhao, and H. Wang, "Calculation of the diffusion coefficient of gas diffusion in coal: The comparison of numerical model and traditional analytical model," J. Pet. Sci. Eng. **205**, 108931 (2021).
3. A. Parekh, G. Chaturvedi, and A. Dutta, "Sustainability analyses of CO2 sequestration and CO2 utilization as competing options for mitigating CO2 emissions," Sustainable Energy Technol. Assessm. **55**, 102942 (2023).
4. H. Wang, Z. G. Qu, and L. Zhou, "A combined GCMC and LBM simulation method for CH4 capture in Cu-BTC particle adsorption bed," Int. Commun. Heat Mass Transfer **88**, 48–53 (2017).
5. S. P. Sullivan, F. M. Sani, M. L. Johns, and L. F. Gladden, "Simulation of packed bed reactors using lattice Boltzmann methods," Chem. Eng. Sci. **60**, 3405–3418 (2005).
6. L. Zhou, Z. G. Qu, L. Chen, and W.-Q. Tao, "Lattice Boltzmann simulation of gas–solid adsorption processes at pore scale level," J. Comput. Phys. **300**, 800–813 (2015).
7. J. Lei, R. Ding, and J. Zhang, "Study on seepage and adsorption characteristics of porous media containing adsorbent based on lattice Boltzmann," AIP Adv. **11**, 045126 (2021).
8. R. Machado, "Numerical simulations of surface reaction in porous media with lattice Boltzmann," Chem. Eng. Sci. **69**, 628–643 (2012).
9. X. Yu, K. Regenauer-Lieb, and F.-B. Tian, "A hybrid immersed boundary-lattice Boltzmann/finite difference method for coupled dynamics of fluid flow, advection, diffusion and adsorption in fractured and porous media," Comput. Geosci. **128**, 70–78 (2019).
10. T. R. Zakirov and M. G. Khramchenkov, "Effect of pore space heterogeneity on the adsorption dynamics in porous media at various convection-diffusion and reaction conditions: A lattice Boltzmann study," J. Pet. Sci. Eng. **212**, 110300 (2022).
11. S. Succi, *The Lattice Boltzmann Equation for Fluid Dynamics and Beyond* (Oxford Univ. Press, UK, 2001).
12. T. R. Zakirov, M. A. Varfolomeev, and C. Yuan, "Characterization of dynamic adsorption regimes in synthetic and natural porous structures using lattice Boltzmann simulations," Chem. Eng. Res. Des. **189**, 14–29 (2023).
13. S. Leclaire, A. Parmigiani, O. Malaspinas, B. Chopard, and J. Latt, "Generalized three-dimensional lattice Boltzmann color-gradient method for immiscible two-phase pore-scale imbibition and drainage in porous media," Phys. Rev. E **95**, 033306 (2017).
14. F. O. Alpak, F. Gray, N. Saxena, J. Dietderich, R. Hofmann, and S. Berg, "A distributed parallel multiple-relaxation-time lattice Boltzmann method on general-purpose graphics processing units for the rapid and scalable computation of absolute permeability from high-resolution 3D micro-CT images," Comput. Geosci. **22**, 815–832 (2018).
15. Q. Kang, P. C. Lichtner, and D. Zhang, "Lattice Boltzmann pore-scale model for multicomponent reactive transport in porous media," J. Geophys. Res. **111**, B05203 (2006).
16. T. R. Zakirov, A. N. Kolchugin, A. A. Galeev, and M. G. Khramchenkov, "Evaluation of absolute permeability in heterogeneous and anisotropic porous media using the lattice boltzmann simulations," Lobachevskii J. Math. **42**, 3048–3055 (2021).